Electronic Supplementary Material (ESI) for Nanoscale.
This journal is © The Royal Society of Chemistry 2021

Supplementary Information for "Two-dimensional Weyl points and nodal lines in pentagonal materials and their optical response"

Sergio Bravo[†1], M. Pacheco[§1], V. Nuñez[1], J.D. Correa[2], and Leonor Chico[⋆3]

[1]Departamento de Física, Universidad Técnica Federico Santa María, Valparaíso, Chile
[2]Facultad de Ciencias Básicas, Universidad de Medellín, Medellín, Colombia
[3]Departamento de Física de Materiales, Facultad de Ciencias Físicas, Universidad Complutense de Madrid, 28040 Madrid, Spain

[†]sergio.bravo.14@sansano.usm.cl
[§]monica.pacheco@usm.cl
[⋆]leochico@ucm.es

Outline: The following supplementary material is divided in two parts. Part A presents extended information for the electronic, dynamical and optical calculations for all the materials presented in the main article. Part B deals briefly with the extension of the space group characterization for multilayer pentagonal structures, with two and three layers.

Part A: Additional information for pentagonal materials

We present further details for the first-principles results related to the novel pentagonal materials proposed in the main article. In particular, the geometric parameters and the band structure with GGA (PBE) and hybrid functionals are reported along with additional spin textures for each material. Also, the phonon band structure is given for the novel materials first proposed in this work. Finally, the optical responses not included in the main article are presented here.

Geometric properties of novel pentagonal materials

The structural parameters were calculated with two first-principles packages: QUANTUM ESPRESSO (QE) [1] and GPAW [2]. The reason for this is the possibility to calculate Wannier-interpolated bands with QE, and on the other side, to employ hybrid functionals as well as to obtain phonon band structures with GPAW. We have checked carefully that both codes give the same electronic band structures for all the materials reported. Although relaxed geometric parameters could differ between the two codes, the difference is under the expected bounds related to the different numerical procedures that are applied. The GPAW relaxed lattice structures for PdSeTe, PdSeS and $GeBi_2$ are depicted in Fig. S.1. The geometric parameters for both QE and GPAW are presented in Table S.1 and Table S.2, respectively.

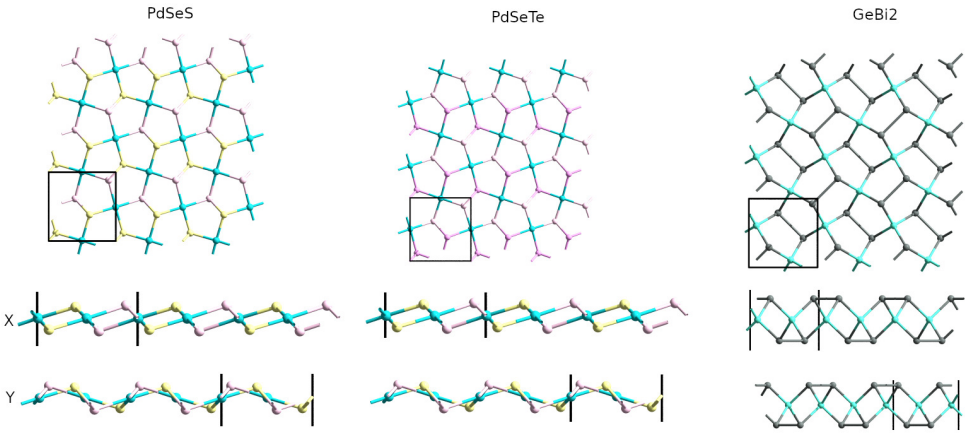

Figure S.1: Lattice structure for the three new pentagonal materials presented in the main article as obtained by GPAW.

Computational details for GPAW calculations

For the electronic structure calculations the real-space projector augmented wavefunction method was employed, [3] together with the atomic simulation environment (ASE) [4, 5]. In order to check the QE results, the first exchange-correlation functional used was a PBE functional [6]. There is a very good agreement between the outcomes of both codes. This gives way to perform further computations with additional features. Thus, additional band structure calculations with a hybrid functional in the form of the HSE06 implementation

Material	**a**(Å)	**b**(Å)	**d**(Å)	**Bonds**(Å)		
PdSeS	5.619	5.754	1.469	**Pd-S**	**Pd-Se**	**Se-S**
				2.351	2.445	2.278
PdSeTe	5.939	6.168	1.663	**Pd-Te**	**Pd-Se**	**Se-Te**
				2.595	2.486	2.604
$GeBi_2$	5.831	5.831	3.558		**Ge-Bi**	
					2.775	

Table S.1: Structural parameters for PdSeS, PdSeTe and $GeBi_2$ extracted from GPAW. $\boldsymbol{a}$ and $\boldsymbol{b}$ are the lattice vectors in the x and y directions, respectively; $\boldsymbol{d}$ is the distance between the bottom and top atoms. The bond length is given in the last column.

Material	**a**(Å)	**b**(Å)	**d**(Å)	**Bonds**(Å)		
PdSeS	5.616	5.752	1.468	**Pd-S**	**Pd-Se**	**Se-S**
				2.350	2.444	2.277
PdSeTe	5.951	6.183	1.664	**Pd-Te**	**Pd-Se**	**Se-Te**
				2.610	2.481	2.608
$GeBi_2$	5.849	5.849	3.500	**Ge-Bi**	**Bi-Bi**	
				2.776	3.016	

Table S.2: Structural parameters for PdSeS, PdSeTe and $GeBi_2$ extracted from QE. $\boldsymbol{a}$ and $\boldsymbol{b}$ are the lattice vectors in the x and y directions, respectively; $\boldsymbol{d}$ is the distance between the bottom and top atoms. The bond length is given in the last column.

[7] were obtained for PdSeS, PdSeTe and $GeBi_2$ as presented in Fig. S.3, Fig. S.10 and Fig. S.18, respectively. The energy cutoff was set to 850 eV and the Brillouin zone was sampled via a $10 \times 10 \times 1$ Monkhorst-Pack k-grid. A vacuum space of 15 Å in the direction normal to the monolayer plane was used and the unit cell was relaxed until the atomic forces were less than 0.01 eV/atom. In addition to these electronic band calculations, we obtained the phonon dispersions. For this we employed a LCAO mode computation [8] with localized double-ζ and single-polarized atomic orbitals, with a $5 \times 5 \times 1$ supercell. Phonon bands for PdSeS, PdSeTe and $GeBi_2$ are depicted in Fig. S.4, Fig. S.11 and S.19, respectively. These results show that all the new materials presented are dynamically stable.

PdSeS information

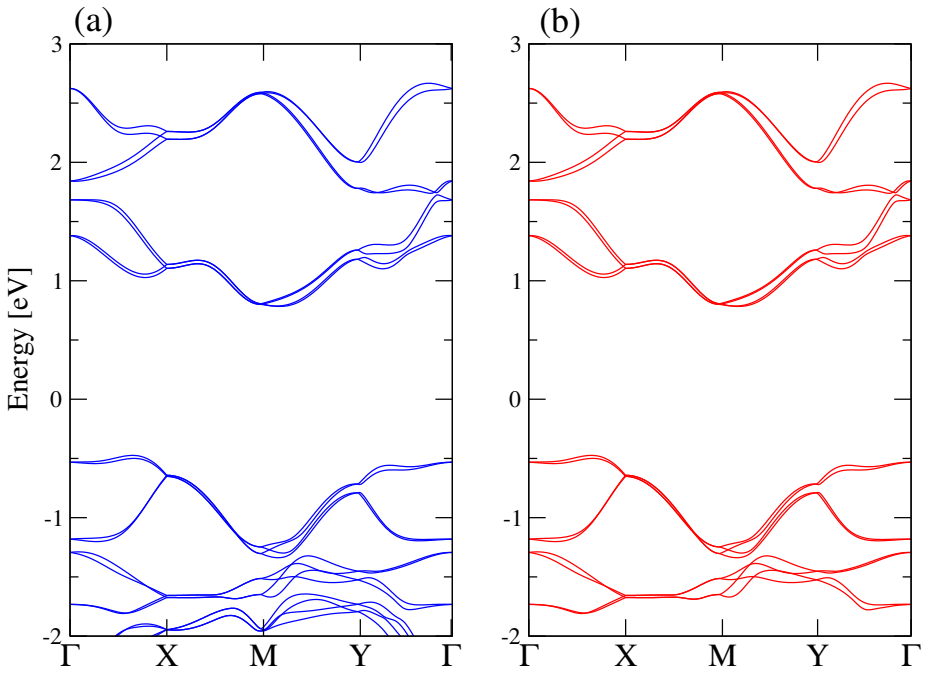

Figure S.2: Electronic band structure for PdSeS from a) QE and b) Wannier interpolation.

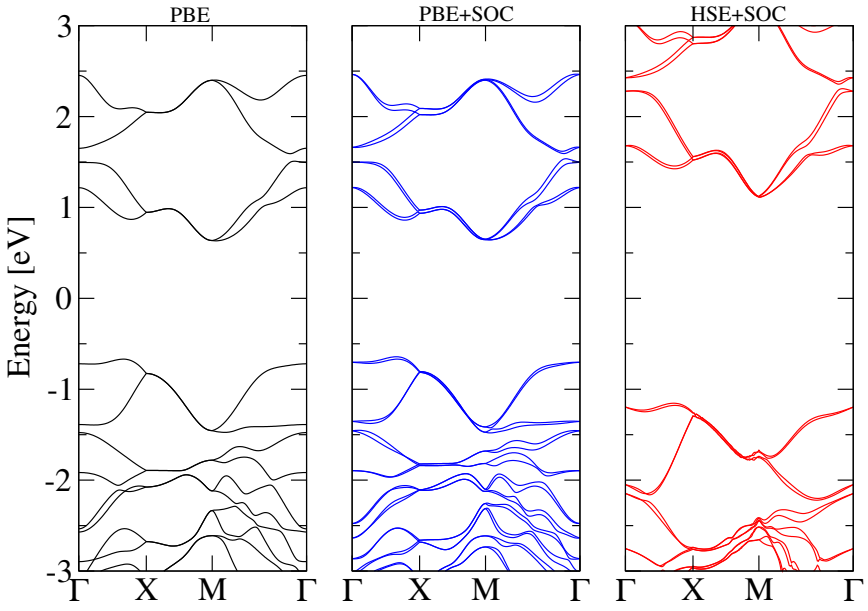

Figure S.3: Electronic band structure for PdSeS obtained with GPAW. Including calculations without SOC, with SOC and the PBE functional and with the hybrid functional with SOC. The results agree very well with those obtained from QE in Fig. S.2.

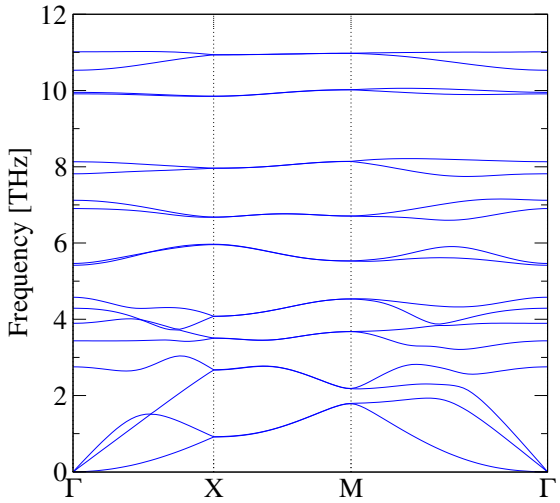

Figure S.4: Phonon band structure for PdSeS from GPAW.

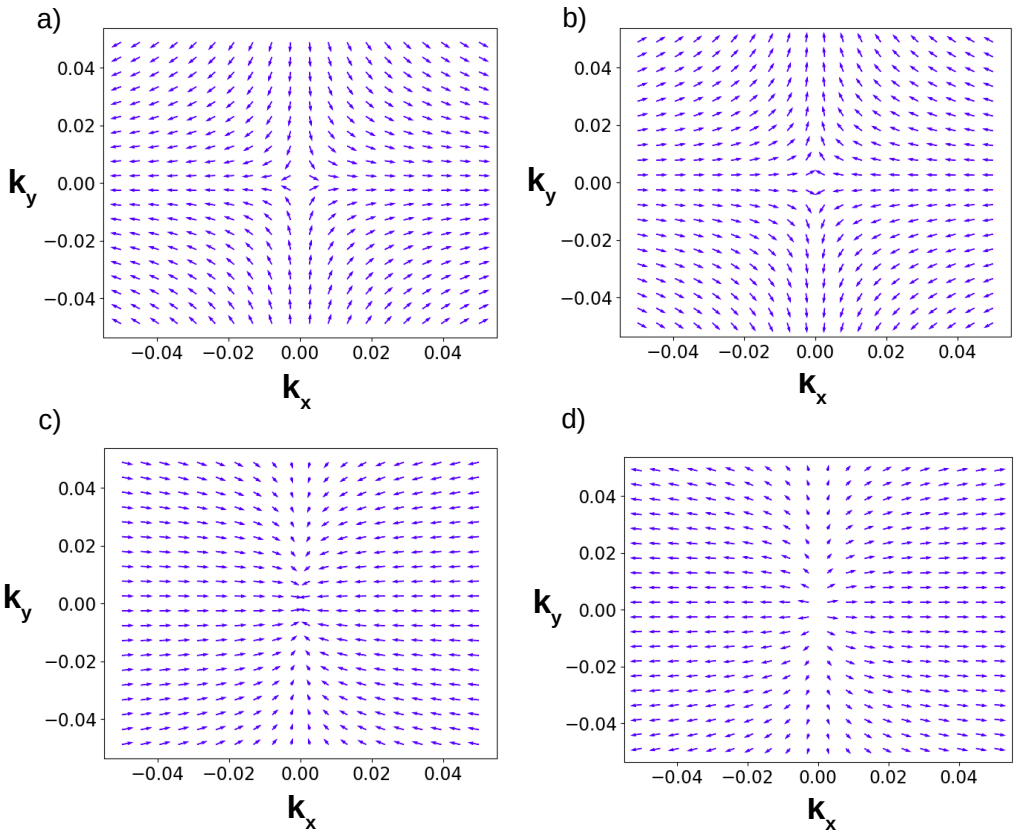

Figure S.5: Spin texture near the Γ point for a) top b) second c) third and d) fourth valence bands for PdSeS.

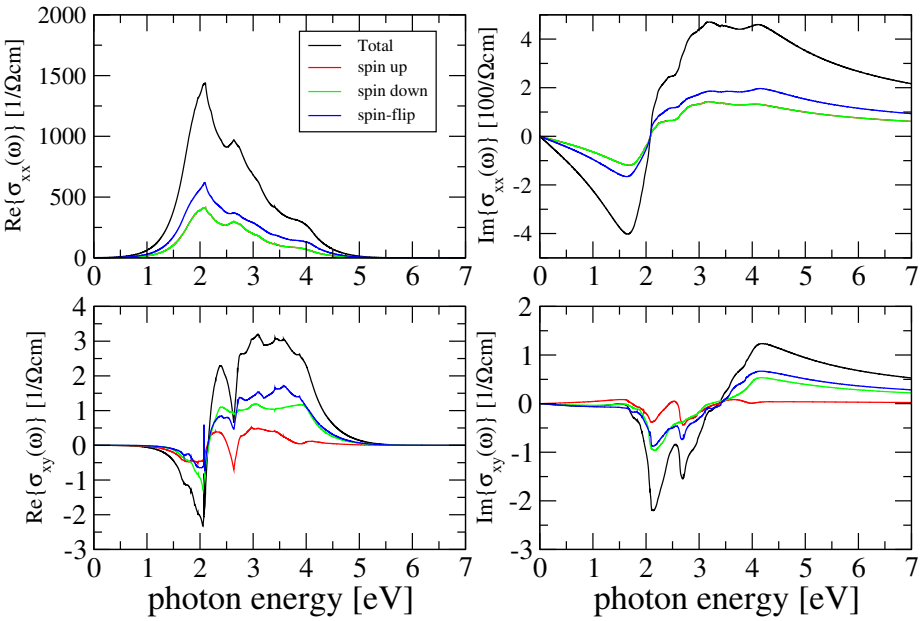

Figure S.6: Optical conductivity with spin-resolved components along the spin x direction for PdSeS. Other directions give similar results.

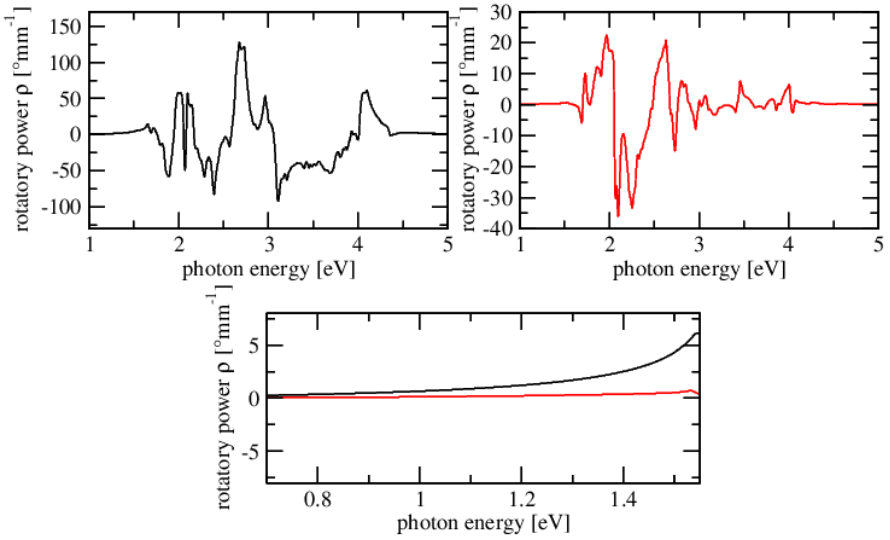

Figure S.7: Natural optical activity in terms of the rotatory power ρ for PdSeS.

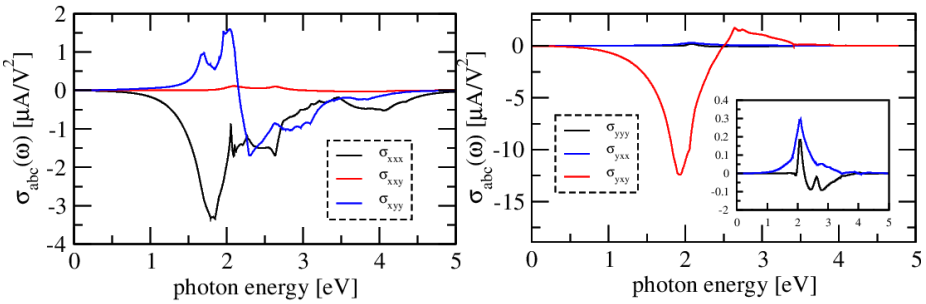

Figure S.8: Nonzero components of the shift current tensor σ_{abc} for PdSeS.

PdSeTe additional information

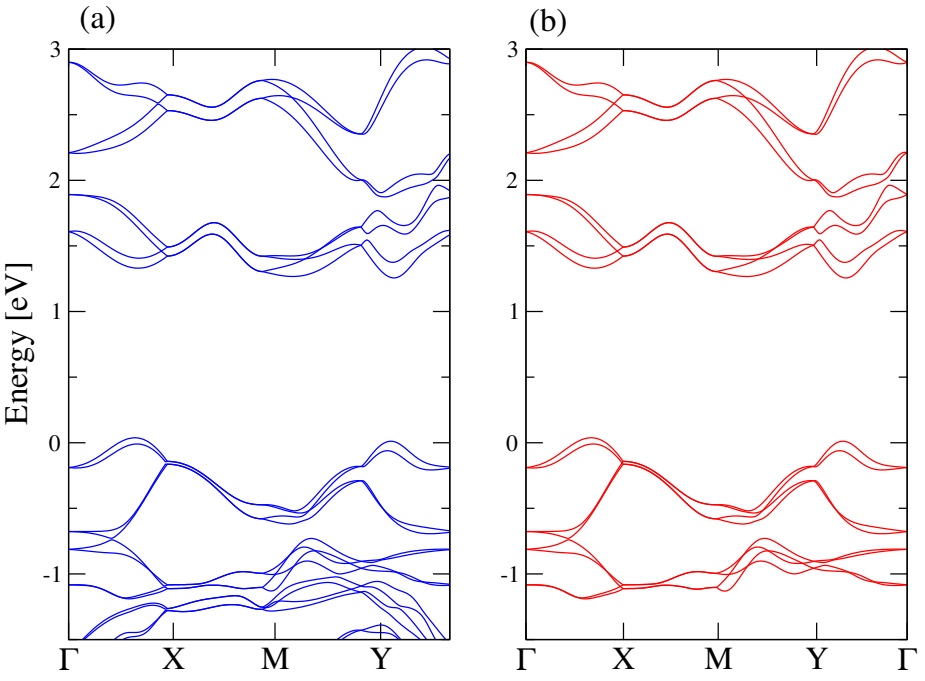

Figure S.9: Electronic band structure for PdSeTe from a) QE and b) Wannier interpolation. The band structure from QE is repeated here for the sake of comparison.

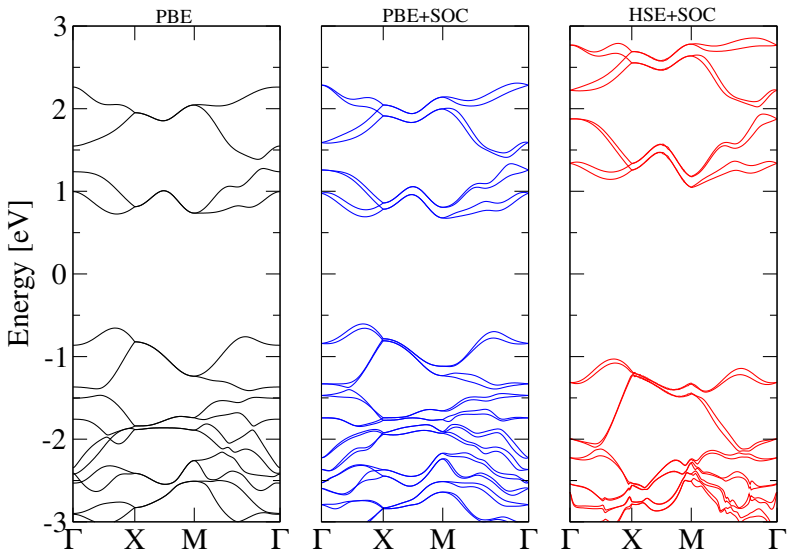

Figure S.10: Electronic band structure for PdSeTe obtained with GPAW. Including calculations without SOC, with SOC and the PBE functional and with the hybrid functional with SOC. The results agree very well with those obtained from QE in Fig. S.9.

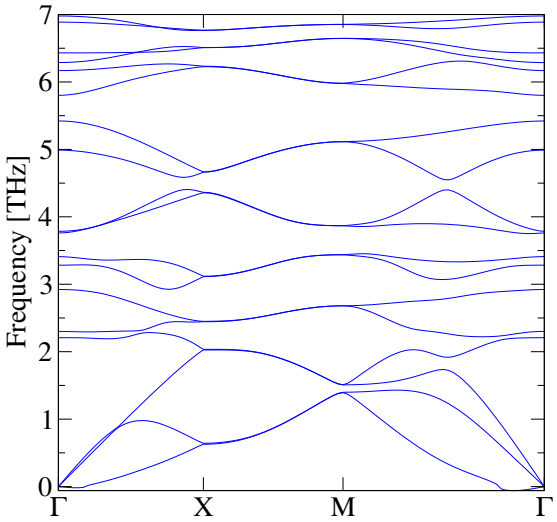

Figure S.11: Phonon band structure for PdSeTe from GPAW.

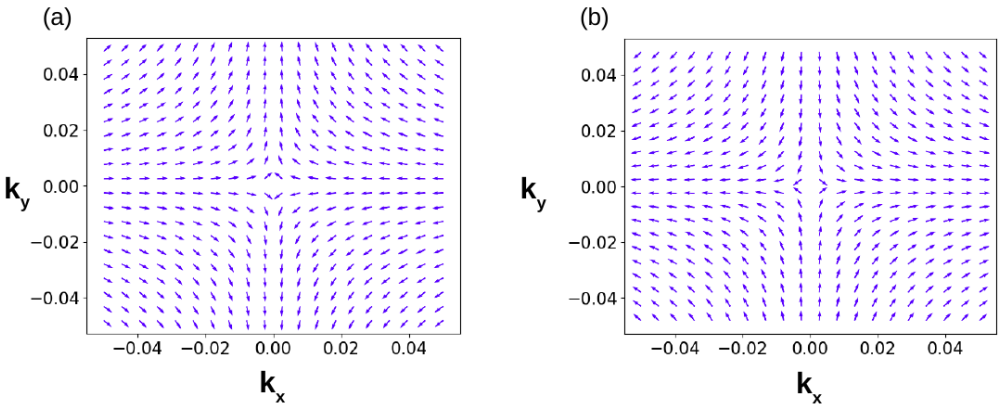

Figure S.12: Spin texture for a) the top valence band and b) the second valence band for PdSeTe.

InP_5 additional information

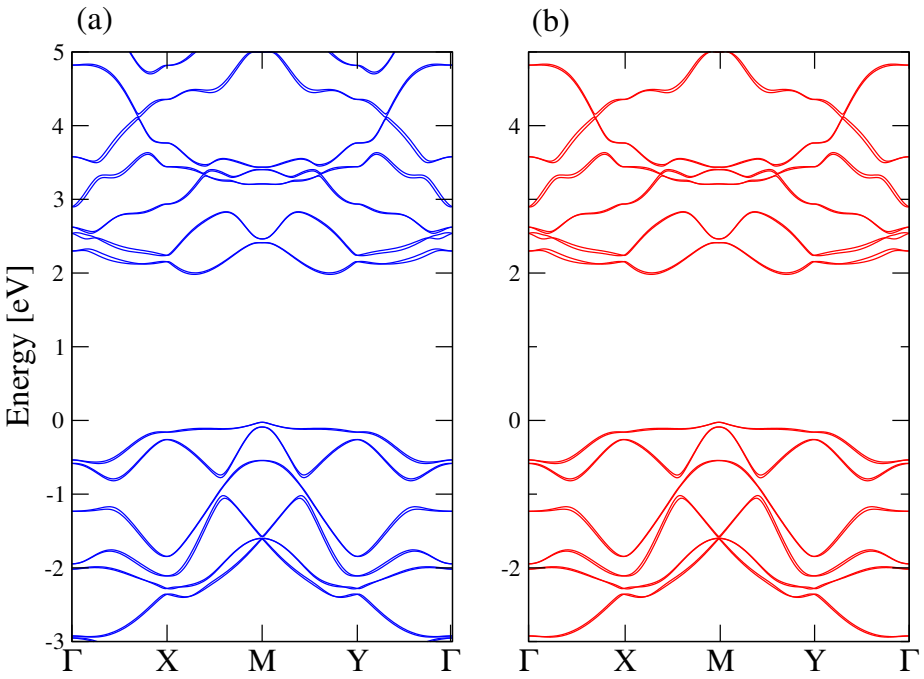

Figure S.13: Electronic band structure for InP_5 from a) QE and b) Wannier interpolation. The band structure from QE has been repeated here to facilitate comparison. This material has been reported elsewhere [9]; therefore, no further calculations are provided for phonons and band structure.

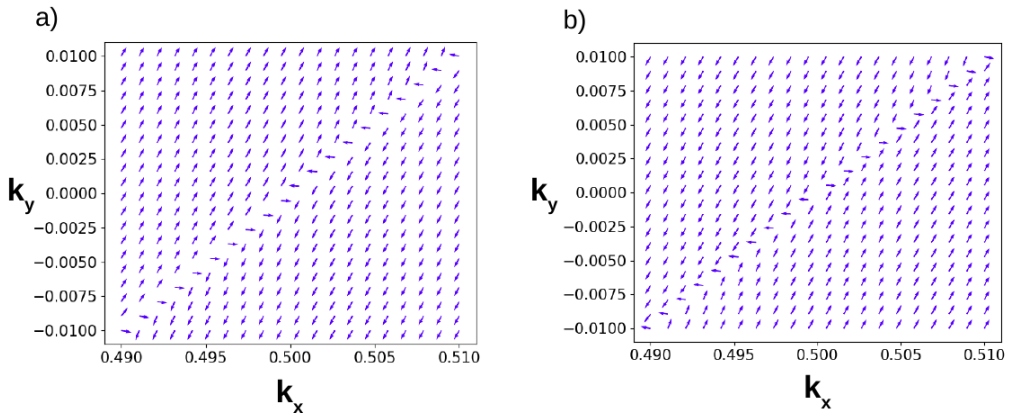

Figure S.14: Spin texture near the X point for a) the top valence band and b) the second uppermost valence band for InP_5.

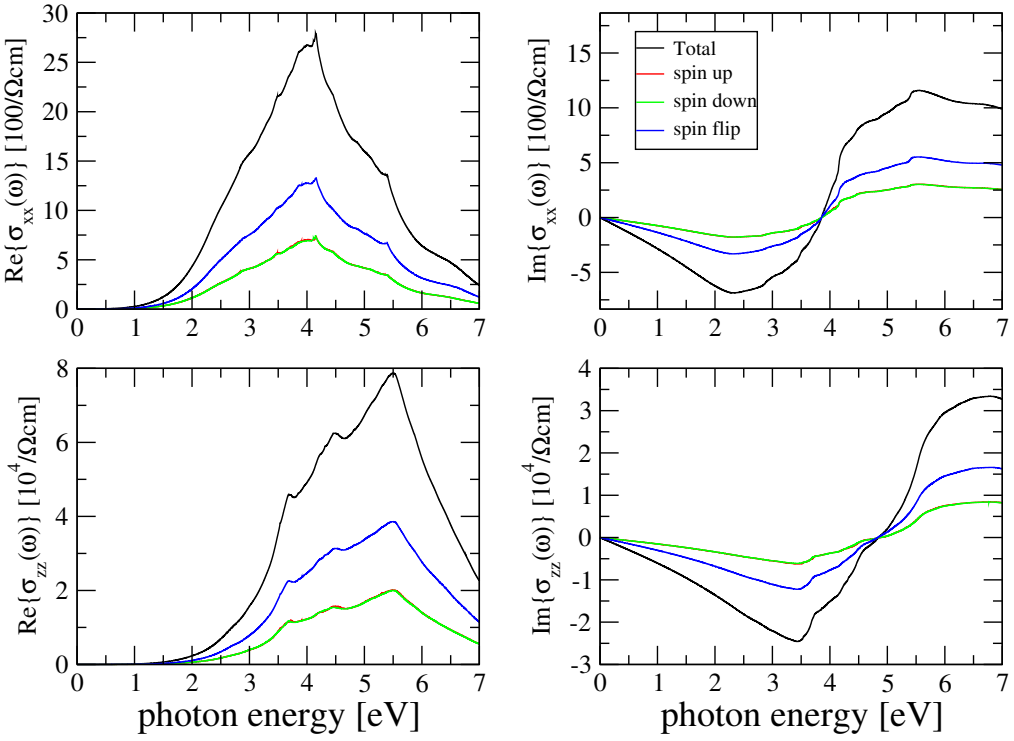

Figure S.15: Optical conductivity with spin-resolved components along the spin z direction for InP_5. Other directions give similar results.

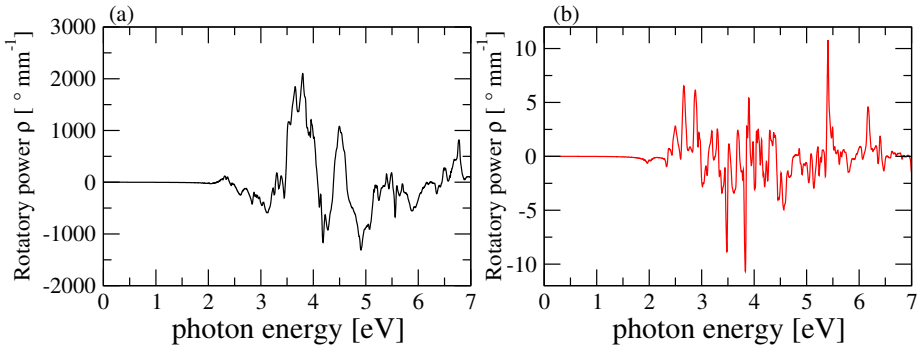

Figure S.16: Natural optical activity in terms of the rotatory power ρ for InP_5.

$GeBi_2$ additional information

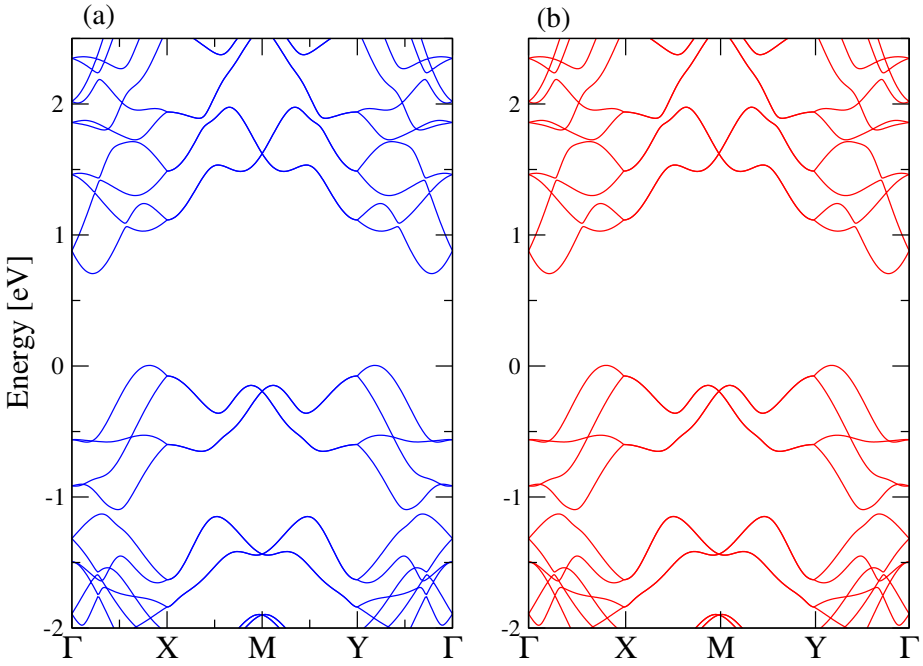

Figure S.17: Electronic band structure for $GeBi_2$ from (a) QE and (b) Wannier interpolation. The band structure from QE has been repeated here to facilitate comparison.

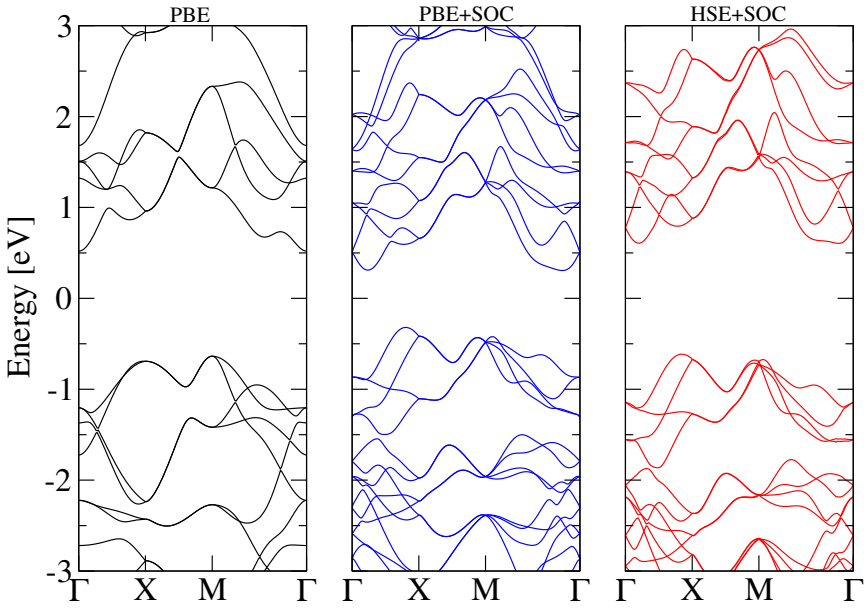

Figure S.18: Electronic band structure for $GeBi_2$ obtained with GPAW. Including calculations without SOC, with SOC and the PBE functional and with the hybrid functional with SOC. The results agree very well with those obtained from QE in Fig. S.17.

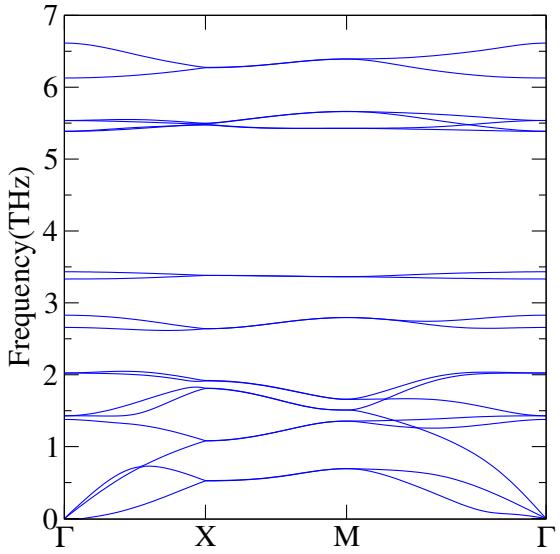

Figure S.19: Phonon band structure for $GeBi_2$ from GPAW.

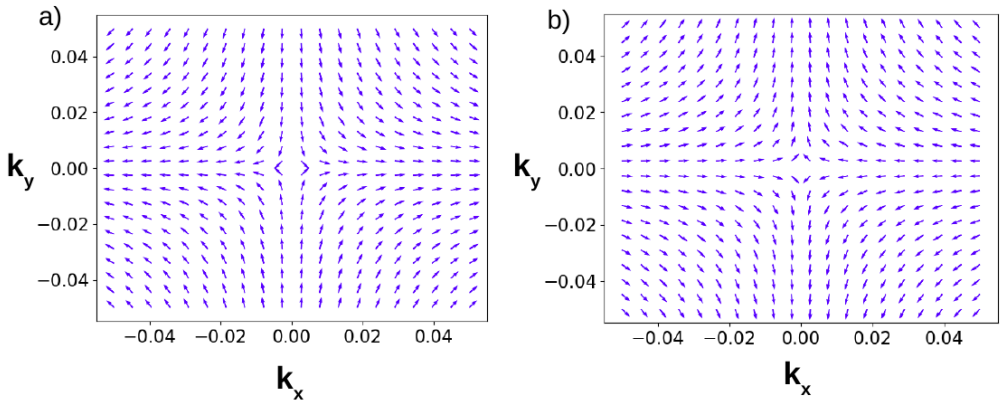

Figure S.20: Spin texture in the Γ point vicinity for a) bottom conduction band b) second conduction band for $GeBi_2$.

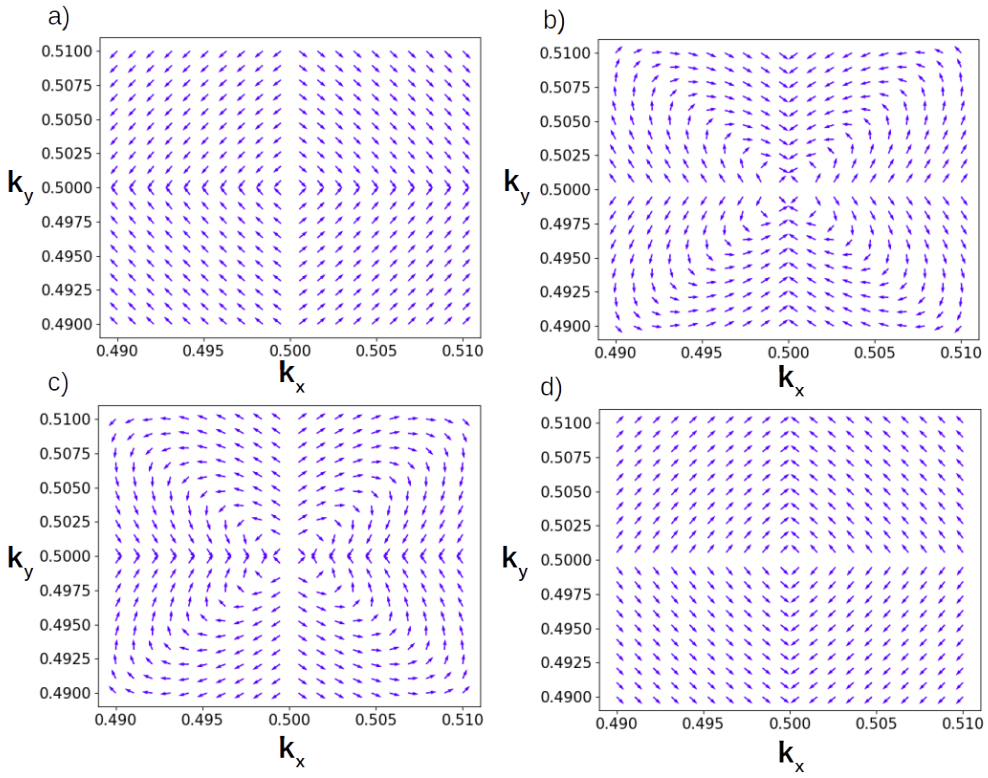

Figure S.21: Spin texture in the neighborhood of the M point for a) top valence band, b) second valence band, c) third valence band and d) fourth valence band for $GeBi_2$. Note that the spin (band) partners are not contiguous for the a) and d) case.

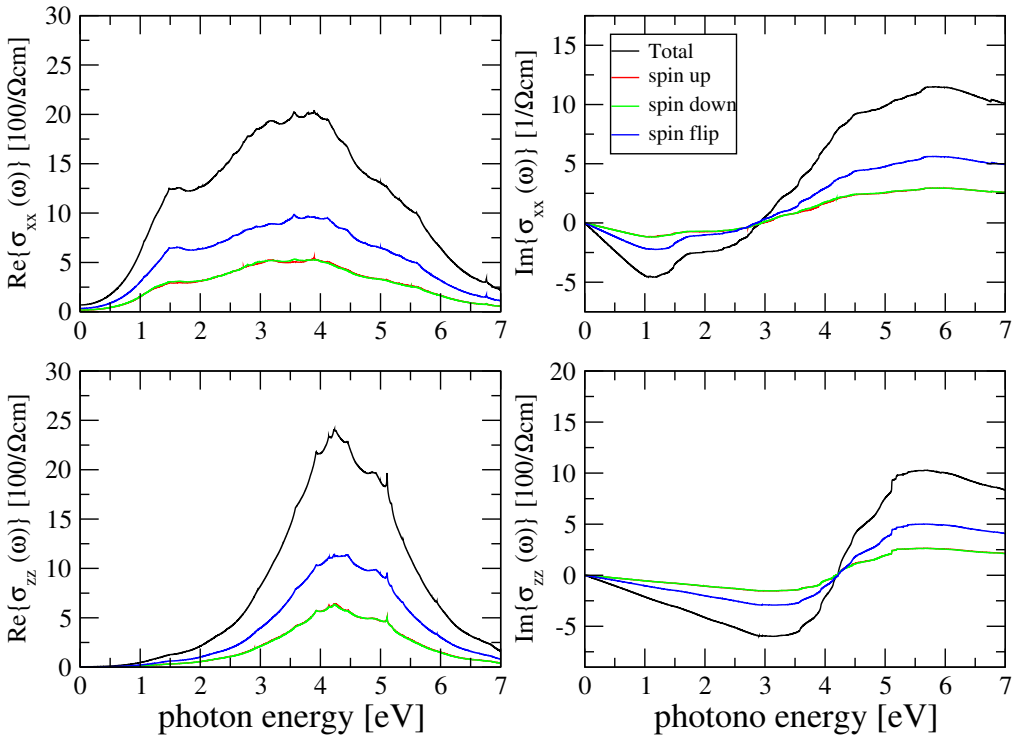

Figure S.22: Optical conductivity with spin-resolved components along the spin z direction for $GeBi_2$. Other directions give similar results.

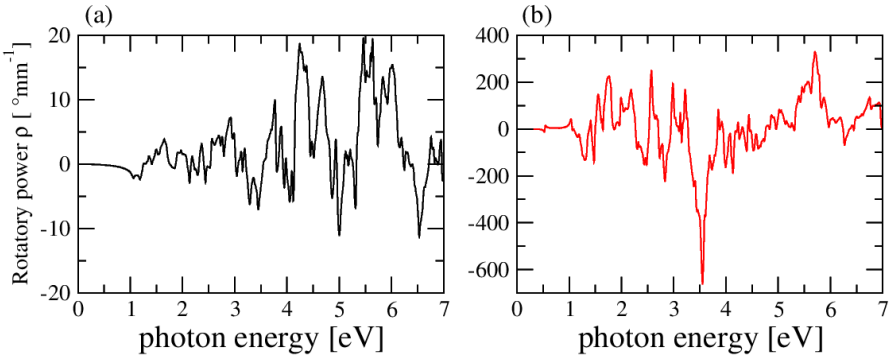

Figure S.23: Natural optical activity in terms of the rotatory power ρ for $GeBi_2$.

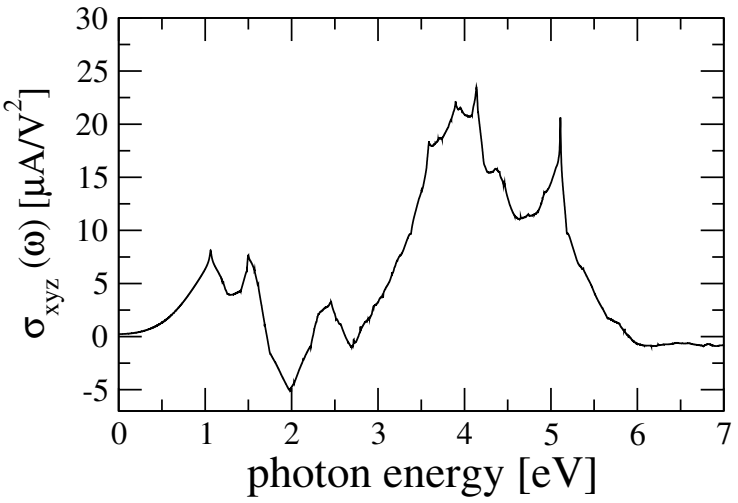

Figure S.24: The nonzero component of the shift current tensor σ_{abc} for $GeBi_2$.

Part B: Multilayer space groups information

Bilayer space groups

The most straightforward way to build multilayer structures is using the so-called slip (translational) stacking. In the bilayer case presented here, two monolayers with the same space group are positioned with a relative displacement described by the vector (t_1,t_2,t_3). We consider the following relative translation vectors for the analysis (in units of the lattice vectors)

- $\tau_1 = (0, 0, t_3)$
- $\tau_{2,1} = (\frac{1}{2}, 0, t_3)$ and $\tau_{2,2} = (0, \frac{1}{2}, t_3)$.
- $\tau_3 = (\frac{1}{2}, \frac{1}{2}, t_3)$.
- $\tau_{4,1} = (\frac{1}{4}, 0, t_3)$ and $\tau_{4,2} = (0, \frac{1}{4}, t_3)$.
- $\tau_5 = (\frac{1}{4}, \frac{1}{4}, t_3)$.
- $\tau_{6,1} = (\frac{1}{2}, \frac{1}{4}, t_3)$ and $\tau_{6,2} = (\frac{1}{4}, \frac{1}{2}, t_3)$.
- $\tau_{7,1} = (t_1, 0, t_3)$ and $\tau_{7,1} = (0, t_2, t_3)$.

For each of these vectors we computed the space group that describes the structure. The calculations were done with the aid of the *spglib* python library [10] and checked with the *FindSym* code [11]. The results of the computation of the space group for each particular stacking are summarized in Table S.3, with the exception of vector $\tau_1 = (0, 0, t_3)$ which yields the same space group as the composing monolayers.

Space group of the monolayer	**Translation vectors**	**Bilayer space group**
$P4/mbm$ (#127*)	$\tau_{2,1}$ and $\tau_{2,2}$	$Pcca$ (#54)
	τ_3	$P4/nbm$ (#125)
	$\tau_{4,1}$ and $\tau_{4,2}$	$P2_1/c$ (#14)
	τ_5	$C2/m$ (#12)
	$\tau_{6,1}$ and $\tau_{6,2}$	$P2/c$ (#13)
	$\tau_{7,1}$ and $\tau_{7,2}$	$P2_1/c$ (#14)
$P\bar{4}2_1m$ (#113)	$\tau_{2,1}$ and $\tau_{2,2}$	$P222_1$ (#17)
	τ_3	$P\bar{4}2m$ (#111)
	$\tau_{4,1}$ and $\tau_{4,2}$	$P2_1$ (#4)
	τ_5	Cm (#8)
	$\tau_{6,1}$ and $\tau_{6,2}$	$P2$ (#3)
	$\tau_{7,1}$ and $\tau_{7,2}$	$P2_1$ (#4)
$P4bm$ (#100)	$\tau_{2,1}$ and $\tau_{2,2}$	$Pba2$ (#32)
	τ_3	$P4bm$ (#100)
	$\tau_{4,1}$ and $\tau_{4,2}$	Pc (#7)
	τ_5	Cm (#8)
	$\tau_{6,1}$ and $\tau_{6,2}$	Pc (#7)
	$\tau_{7,1}$ and $\tau_{7,2}$	Pc (#7)
$P42_12$ (#90)	$\tau_{2,1}$ and $\tau_{2,2}$	$P222_1$ (#17)
	τ_3	$P422$ (#89)
	$\tau_{4,1}$ and $\tau_{4,2}$	$P2_1$ (#4)
	τ_5	$C2$ (#5)
	$\tau_{6,1}$ and $\tau_{6,2}$	$P2$ (#3)
	$\tau_{7,1}$ and $\tau_{7,2}$	$P2_1$ (#4)
$Pbam$ (#55)	$\tau_{2,1}$ and $\tau_{2,2}$	$Pcca$ (#54)
	τ_3	$Pban$ (#50)
	$\tau_{4,1}$ and $\tau_{4,2}$	$P2_1/c$ (#14)
	τ_5	$P\bar{1}$ (#2)
	$\tau_{6,1}$ and $\tau_{6,2}$	$P2/c$ (#13)
	$\tau_{7,1}$ and $\tau_{7,2}$	$P2_1/c$ (#14)
$Pba2$ (#32)	$\tau_{2,1}$ and $\tau_{2,2}$	$Pba2$ (#32)
	τ_3	$Pba2$ (#32)
	$\tau_{4,1}$ and $\tau_{4,2}$	Pc (#7)
	τ_5	$P1$ (#1)
	$\tau_{6,1}$ and $\tau_{6,2}$	Pc (#7)
	$\tau_{7,1}$ and $\tau_{7,2}$	Pc (#7)
$P2_12_12$ (#18)	$\tau_{2,1}$ and $\tau_{2,2}$	$P222_1$ (#17)
	τ_3	$P2$ (#3)
	$\tau_{4,1}$ and $\tau_{4,2}$	$P2_1$ (#4)
	τ_5	$P1$ (#1)
	$\tau_{6,1}$ and $\tau_{6,2}$	$P2$ (#3)
	$\tau_{7,1}$ and $\tau_{7,2}$	$P2_1$ (#4)
$P2_1/c$ (#14)	$\tau_{2,1}$ and $\tau_{2,2}$	$P2/c$ (#17) and $P2_1/c$ (#14)
	τ_3	$P2/c$ (#13)
	$\tau_{4,1}$ and $\tau_{4,2}$	$P1$ (#1) and $P2_1/c$ (#14)
	τ_5	$C2$ (#5)
	$\tau_{6,1}$ and $\tau_{6,2}$	$P2$ (#3)
	$\tau_{7,1}$ and $\tau_{7,2}$	$P1$ (#1)

Table S.3: Space groups for bilayer pentagonal structures based on the monolayers space groups. *The SG #117 gives the same groups as the same WP coordinates are used for both groups.

Frequency tables for the case with $n = 3$ layers

When we add a third layer to the system, the stacking combinations increase substantially, implying that the enumeration of the space groups for these configurations becomes cumbersome and fairly impractical. Evidently this extends to $n > 3$. Despite that, we can do a general analysis for some space groups chosen as examples. We select SG #127 and SG #113, whose multilayers could be of interest due to great number of reported materials belonging to these two space groups. We present in Fig. S.25 and Fig. S.26 a summary for parent SG #127 and SG #113, respectively, in the form of two frequency charts that show the most recurring space groups arising from the stackings defined above.

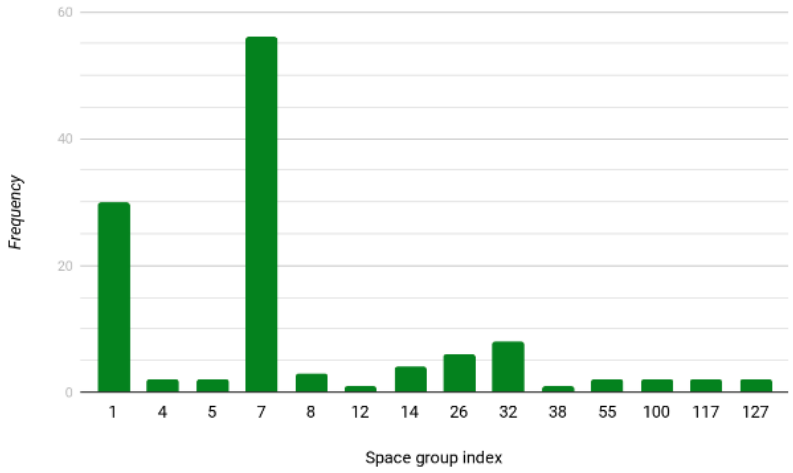

Figure S.25: Frequency graph for the possible space groups that can be formed by translational stacking of SG #127 monoloyers.

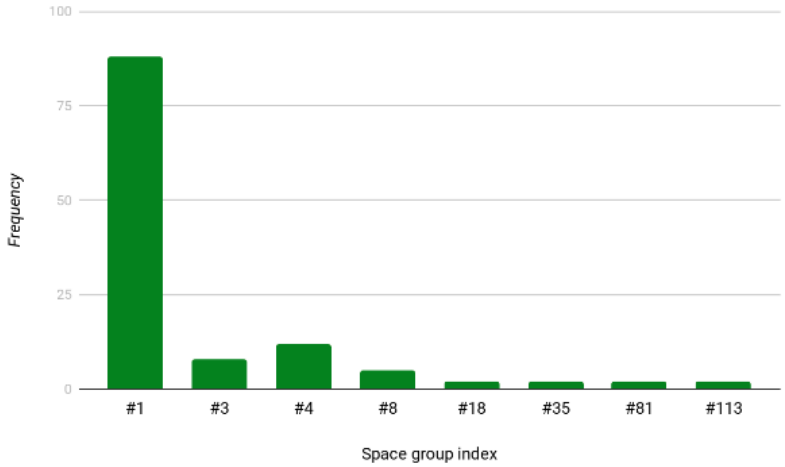

Figure S.26: Frequency graph for the possible space groups that can be formed by translational stacking of SG #113 monoloyers.

It can be noted in Fig. S.25 that for the space group #127, the most frequent three-layer group is #7. This is in contrast with what is is generally expected; that the #1 space group dominates the frequency count, as happens for example with space group #113 in Fig. S.26.

The above procedure can be easily continued for $n > 3$ but in general the trivial space group $P1$, will have an even greater incidence.

References

[1] Paolo Giannozzi, Oscar Baseggio, Pietro Bonfà, Davide Brunato, Roberto Car, Ivan Carnimeo, Carlo Cavazzoni, Stefano de Gironcoli, Pietro Delugas, Fabrizio Ferrari Ruffino, Andrea Ferretti, Nicola Marzari, Iurii Timrov, Andrea Urru, and Stefano Baroni. Quantum ESPRESSO toward the exascale. *The Journal of Chemical Physics*, 152(15):154105, 2020.

[2] JE Enkovaara, Carsten Rostgaard, J Jørgen Mortensen, Jingzhe Chen, M Dułak, Lara Ferrighi, Jeppe Gavnholt, Christian Glinsvad, V Haikola, HA Hansen, et al. Electronic structure calculations with gpaw: a real-space implementation of the projector augmented-wave method. *Journal of Physics: Condensed Matter*, 22(25):253202, 2010.

[3] Jens Jørgen Mortensen, Lars Bruno Hansen, and Karsten Wedel Jacobsen. Real-space grid implementation of the projector augmented wave method. *Physical Review B*, 71(3):035109, 2005.

[4] S. R. Bahn and K. W. Jacobsen. An object-oriented scripting interface to a legacy electronic structure code. *Comput. Sci. Eng.*, 4(3):56–66, 2002.

[5] Ask Hjorth Larsen, Jens Jørgen Mortensen, Jakob Blomqvist, Ivano E Castelli, Rune Christensen, Marcin Dułak, Jesper Friis, Michael N Groves, Bjørk Hammer, Cory Hargus, Eric D Hermes, Paul C Jennings, Peter Bjerre Jensen, James Kermode, John R Kitchin, Esben Leonhard Kolsbjerg, Joseph Kubal, Kristen Kaasbjerg, Steen Lysgaard, Jón Bergmann Maronsson, Tristan Maxson, Thomas Olsen, Lars Pastewka, Andrew Peterson, Carsten Rostgaard, Jakob Schiøtz, Ole Schütt, Mikkel Strange, Kristian S Thygesen, Tejs Vegge, Lasse Vilhelmsen, Michael Walter, Zhenhua Zeng, and Karsten W Jacobsen. The atomic simulation environment—a python library for working with atoms. *Journal of Physics: Condensed Matter*, 29(27):273002, 2017.

[6] John P Perdew, Kieron Burke, and Matthias Ernzerhof. Generalized gradient approximation made simple. *Physical Review Letters*, 77(18):3865, 1996.

[7] Jochen Heyd, Gustavo E Scuseria, and Matthias Ernzerhof. Hybrid functionals based on a screened coulomb potential. *The Journal of Chemical Physics*, 118(18):8207–8215, 2003.

[8] A. H. Larsen, M. Vanin, J. J. Mortensen, K. S. Thygesen, and K. W. Jacobsen. Localized atomic basis set in the projector augmented wave method. *Phys. Rev. B*, 80(19):195112, 2009.

[9] Mosayeb Naseri. Investigation on the stability and electronic properties of penta-xp5 (x=al, ga, in) monolayer semiconductors by using first principles calculations. *Chemical Physics Letters*, 706:99–106, 2018.

[10] Atsushi Togo and Isao Tanaka. `Spglib`: a software library for crystal symmetry search. *arXiv e-prints*, page arXiv:1808.01590, August 2018.

[11] Harold T. Stokes and Dorian M. Hatch. *FINDSYM*: program for identifying the space-group symmetry of a crystal. *Journal of Applied Crystallography*, 38(1):237–238, Feb 2005.